An Analytical Model for Coherent Transmission Performance Estimation After Generic Jones Matrices

# An Analytical Model for Coherent Transmission Performance Estimation after Generic Jones Matrices

Giuseppe Rizzelli, Pablo Torres-Ferrera, and Roberto Gaudino, *Senior Member, IEEE*

***Abstract*—In this paper, we propose the extension of a previously presented analytical model for the estimation of the signal-to-noise ratio (SNR) at the output of an adaptive equalizer in polarization multiplexed (PM)-QAM coherent optical systems when transmission is modeled as a generic 2x2 frequency dependent transfer function matrix. We present the model and then we statistically test its accuracy in two possible application environments. Our findings show a remarkable agreement between time-domain simulations and analytical results, with average SNR discrepancies of the order of 0.1 dB. We believe our model can find important applications in next generation physical layer aware network planning tools that need to take into account polarization dependent loss/gain and strong filtering, for instance in ultra high baud rate coherent systems.**

***Index Terms*—Coherent Detection, Optical Communications, Performance Modelling.**

## I. Introduction

COHERENT detection (CoD) coupled with digital signal processing (DSP) is the ultimate choice in modern high-speed metro and long-haul optical communications networks [1], [2], and may soon be introduced also in access and short reach networks [3], [4]. CoD systems rely on advanced modulation formats to achieve very high bitrates by taking advantage of three main coherent signal features: intensity, phase and polarization. At the receiver side, sophisticated DSP algorithms are required to compensate for the (linear and nonlinear) impairments introduced by the optical transmission channel, implementing clock recovery, carrier phase recovery, polarization recovery and adaptive feed-forward equalization (FFE) [5]. In several situations, such as for physical layer-aware optical network dimensioning using software planning tools [6], ultra-fast numerical estimation of physical layer performance is needed. Typically, the estimation is based on the available optical signal to noise ratio ($OSNR$) at the input of the receiver and on the resulting electrical SNR ($SNR_e$) at the output of the FFE equalizer, the latter being then directly related to the system BER. The relation between $OSNR$ and $SNR_e$ is trivial for frequency flat channels [7]. However, this relation becomes analytically more complex when there is a frequency dependence on the optoelectronics (for instance due to optical frequency-selective filters/switches and/or electrical bandwidth limitations in ultra high baud rate transceivers) and, even more, when polarization dependent effects are present. In simulation, the output $SNR_e$ can be estimated with good accuracy through time-domain simulations that consider also the details of the DSP [5]. Nevertheless, in some applications this approach is too CPU-time consuming, for instance in physical-layer aware real-time network optimization simulations requiring multi-dimensional Monte-Carlo parameters sweeps [8]. In this paper, we thus present an analytical model that allows to obtain $SNR_e$ estimation at the output of the coherent receiver DSP assuming:

- PM-QAM transmission
- a linear transmission channel, with a generic 2x2 frequency-dependent transfer function matrix $\boldsymbol{H}_s(f)$. Thanks to the properties of coherent systems, both optical and electrical bandwidth limitations can be taken into account in a single equivalent $\boldsymbol{H}_s(f)$ matrix.
- colored (i.e. frequency-dependent) additive Gaussian noise at the receiver
- a coherent receiver implementing typical DSP algorithms, and in particular including an FFE equalizer that compensates for polarization and frequency-dependent effects.

We note that in several performance assessments in long-haul network dimensioning, such as in [6], this is the common situation. In fact, thanks to the well-known Gaussian-Noise models [9], fiber non-linearities are modelled through additive Gaussian noise at the receiver, while signal propagation is considered linear.

For a single polarization QAM transmission, a solution is already available in the literature thanks to the analytical tool described in [10]. This model assumes an infinitely long linear minimum mean-squared error (MMSE) equalizer and computes the achievable $SNR_e$ at the equalizer output as a function of the spectral signal-to-noise ratio at the receiver input (sometimes indicated as "channel SNR function" [11]). In this manuscript we extend this approach to make it applicable to PM-QAM, i.e. to a generic polarization multiplexed transmission on a channel including both frequency and polarization dependence for both the signal and the additive noise. After presenting our proposed model, we validate it against time domain simulations over realistic optical network scenarios. In order to find a proper trade-off between implementation complexity and computation speed, as required in physical layer aware network planning tools, we do not explicitly consider non-ideal characteristics such as Kerr effects, chromatic dispersion and transceiver hardware-imposed

G. Rizzelli is with the LINKS Foundation, Torino, Italy, e-mail: giuseppe.rizzelli@linksfoundation.com.

P. Torres-Ferrera and R. Gaudino are with the Department of Electronics and Telecommunications, Politecnico di Torino, Torino, Italy.

This article has been accepted for publication in IEEE/OSA Journal of Lightwave Technology. This is the author's version which has not been fully edited and content may change prior to final publication. Citation information: DOI 10.1109/JLT.2023.3242329



limitations, focusing only on the channel and noise frequency and polarization features. In fact, a more sophisticated model would also require specifying a much larger set of parameters (such as all the second-order details of transceivers, like IQ skews, IQ imbalances, IQ crosstalk in both Tx and Rx), and this would likely go against what is typically required in fast and efficient software network planning tools.

The reminder of this manuscript is organized as follows: in Section II we describe the analytical model while in Section III we address its accuracy by presenting two application scenarios. First, we evaluate a "mainstream" core-network example, where ten optical filters are cascaded together with optical amplifiers to emulate long distance transmission using Reconfigurable Optical Add-Drop Multiplexers (ROADMs). Then, in order to show the applicability of our method also in short-reach optical links, we consider a more exotic example we recently presented in [12], where we studied a multi mode fiber (MMF) unamplified coherent system for future short-reach networks. In both cases, we compare the performance estimation obtained with the analytical model versus detailed time-domain simulations on a PM-16QAM signal. In Section IV we discuss the implications of the presented results and draw some conclusions.

## II. The Proposed Analytical Model

In long-haul optically amplified coherent systems, the relevant noise sources are typically additive Gaussian on the received $\hat{x}$ and $\hat{y}$ optical fields, due to the accumulation of (possibly polarization and frequency dependent) optical amplifier ASE noises. As previously mentioned, even in presence of fiber non-linearities, it is quite typical to model core network transport through the well known Gaussian-Noise models [9], where again the equivalent noise introduced by non-linearities is additive and Gaussian. Moreover, also for coherent short-reach links without optical amplification, as we show for instance in [3], the relevant noise (typically a combination of shot noise and trans-impedance amplifier thermal noise) is to a good approximation again Gaussian and additive on the four electrical signals proportional to the $\hat{x}$ and $\hat{y}$ optical fields and in general frequency-dependent and possibly polarization dependent (for instance when the four electrical gains inside the coherent receiver are not identical). Similarly, in a coherent system (contrary to direct detection) both optical and electrical filtering can be modelled as frequency and possibly polarization dependent transfer functions acting on the transmitted signal. The system we want to study can thus be numerically simulated as the cascade of the following elements:

1) a PM-QAM transmitter generating the signal $\vec{E}_{TX}(t)$;
2) an optical propagation link that can be modelled as a totally generic [2x2] frequency and polarization dependent transfer function $\boldsymbol{H}_s(f)$ acting on the transmitted PM-QAM signal;
3) a coherent receiver acting on $\vec{E}_{RX}(t) = \boldsymbol{H}_s(f)\vec{E}_{TX}(t) + \vec{n}(t)$, where $\vec{n}(t)$ is the additive Gaussian noise (possibly non-flat and, again, polarization dependent).
4) a receiver that compensate for the impact of $\boldsymbol{H}_s(f)$ on signal distortion using a Minimum Mean-Square Error (MMSE)-based FFE-equalizer.

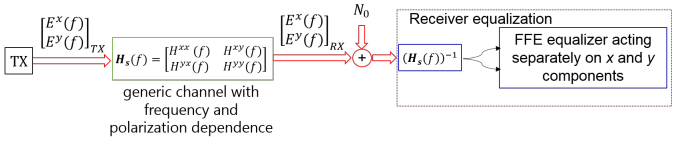


Fig. 1. Block diagram of the system under investigation with white noise.

To predict the system performance, starting from a certain end-to-end transfer function, we can use the analytical model presented in [10], derived under the assumption of additive white Gaussian noise (AWGN) channel with a generic transfer function $H_c(f)$. In [10] the $SNR$ at the output of an infinitely long adaptive MMSE equalizer is computed from the spectrally resolved $SNR(f)$ at the receiver input (in the single polarization case) as:

$$SNR = \frac{1}{T \cdot \int_{-\frac{1}{2T}}^{\frac{1}{2T}} \frac{1}{\overline{SNR}(f)+1} df} \tag{1}$$

where $T$ is the symbol period (i.e. the inverse of the baud rate) and $\overline{SNR}(f)$ is the folded version of the spectral $SNR(f)$, defined as:

$$\overline{SNR}(f) = \sum_{\mu} SNR(f - \frac{\mu}{T}) \tag{2}$$

The spectral $SNR(f)$ is then defined as:

$$SNR(f) = \frac{T\sigma_a^2 |H_T(f)H_C(f)|^2}{N_0(f)} \tag{3}$$

where $\sigma_a^2$ is the transmitted signal power, $H_C(f)$ is the channel transfer function, $H_T(f)$ is the transfer function of the transmitter shaping filter (meaning that the transmitted useful signal power spectral density is proportional to $\sigma_a^2 \cdot |H_T(f)|^2$, which is typically, but not necessarily, a squared root raised cosine filter in PM-QAM transmission), and $N_0(f)$ is the equivalent noise power spectral density at the input of the receiver.

Our goal is to apply this approach to PM transmission and to generic polarization and frequency dependent channels. To present our model, we start from a first somehow simplified situation in which we assume that the additive noise is frequency flat, an assumption we will then remove shortly after. We thus consider the receiver schematic shown in Fig. 1. Then, our first model extension consists on including a generic [2x2] transfer function matrix $\boldsymbol{H}_s(f)$, thus being able to describe any possible linear optical channel according to the following equations:

$$\begin{bmatrix}E^x(f)\\E^y(f)\end{bmatrix}_{RX} = \boldsymbol{H}_s(f) \cdot \begin{bmatrix}E^x(f)\\E^y(f)\end{bmatrix}_{TX} \tag{4}$$

where:

$$\boldsymbol{H}_s(f) = \begin{bmatrix}H_s^{xx}(f) & H_s^{xy}(f)\\H_s^{yx}(f) & H_s^{yy}(f)\end{bmatrix} \tag{5}$$

In the rest of this Section, we will use several times the following well-known result, demonstrated for instance in [13]: in a schematic such as the one shown in Fig. 1 and when using an optimal detection receiver, the resulting performance

This article has been accepted for publication in IEEE/OSA Journal of Lightwave Technology. This is the author's version which has not been fully edited and content may change prior to final publication. Citation information: DOI 10.1109/JLT.2023.3242329



(for instance in terms of output $SNR$ or $BER$) does not change if a linear and invertible operation is applied in the block diagram *after* the summing point between the received signal and the noise. In our case, this basically means that any frequency dependent matrix placed *after* the summing point, provided that it is an invertible matrix at any frequency, will not change the performance.

In our following derivation for Fig. 1, we thus assume that the $\boldsymbol{H}_s(f)$ matrix is invertible inside the useful signal bandwidth, an assumption that in practical system is always satisfied since it basically requires only that $\boldsymbol{H}_s(f)$ does not go to zero inside the useful signal bandwidth. Then, *only* for the target of analytical performance estimation, we consider that the receiver FFE has the following structure:

- A first 2x2 stage $\boldsymbol{H}_s(f)^{-1}$ that compensates the polarization rotation introduced by the channel Jones matrix at each frequency. As previously explained, since this matrix is added *after* the summing point, it will not change the performance. At the output of this block, the two transmitted PM signals are thus re-aligned on the proper $\hat{x}$ and $\hat{y}$ axis, without mutual crosstalk. In practical coherent receiver DSP implementations, this is achieved through a multi input multi output (MIMO) adaptive FFE equalizer.
- then, since polarization crosstalk has been removed, we can assume that FFE is separately applied on each of the two PM components and, consequently, we can apply Eq. 3 independently on the two $\hat{x}$ and $\hat{y}$ QAM components to predict system performance.

These two steps introduce the key idea of our model. Nevertheless, in practical situations a slightly more complex situation is relevant, since also the additive noise power spectral density (PSD) may be non flat, but shaped for instance by ROADMs or other filtering elements. Furthermore, also the noise can be affected by polarization dependent loss (PDL), introduced for instance by slight polarization asymmetries in the EDFA noise figures (or again in the ROADMs). We thus now introduce our second model extension to take into account the more general schematic presented in Fig. 2(a), where $\boldsymbol{H}_s(f)$ takes again into account the linear distortions affecting the useful signal, while $\boldsymbol{H}_n(f)$ allows to consider a generic polarization-dependent PSD for the additive noise. These two frequency-dependent Jones matrixes are, in general, different, since the signal and the noise can see different transfer functions.

In the following and as shown step-by-step in Fig. 2, we introduce several block-diagrams that are all equivalent for what concerns the performance to Fig. 2(a) but at the end of the derivation will allow again to apply Eq. 3 independently on the two $\hat{x}$ and $\hat{y}$ QAM components to predict PM-QAM system performance.

As a first step, shown in Fig. 2(b) and using the aforementioned property of adding an invertible matrix , we introduce the noise-whitening matrix $\boldsymbol{H}_n^{-1}(f)$ after the summing point. In the next step, applying obvious rules on the cascade of linear elements, we can obtain the new equivalent model in Fig. 2(c) where $\boldsymbol{H}_{sn}(f) = \boldsymbol{H}_s(f) \cdot \boldsymbol{H}_n(f)^{-1}$. Then, in order to separate the $\hat{x}$ and $\hat{y}$ QAM components, we can use again

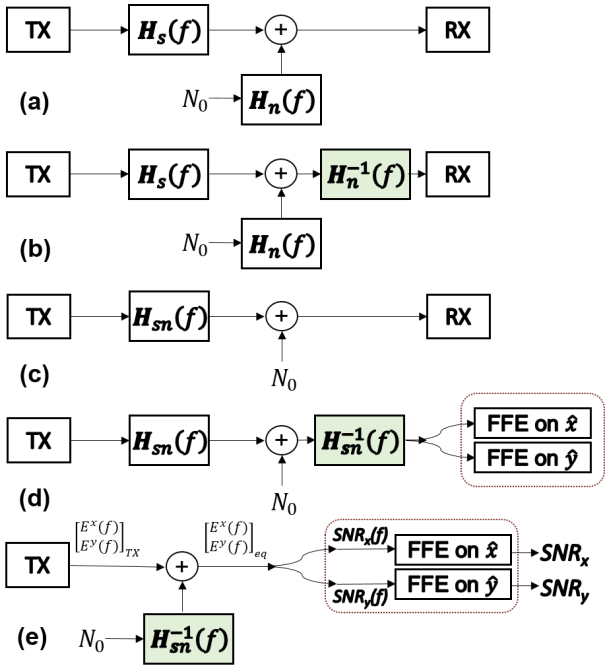


Fig. 2. Extension of the block diagram presented in Fig 1 to take also into account colored and polarization dependent noise PSD, as shown in (a). The block diagrams (b)-(e) are performance-wise equivalent to (a), showing the steps to derive our analytical model.

the invertible operator rule and introduce the matrix $\boldsymbol{H}_{sn}(f)^{-1}$ after the summing point, as shown in Fig. 2(d).

Finally, by considering again the cascade of the linear elements affecting the signal and the noise, we can derive the last equivalent block diagram of Fig. 2(e), which is the final goal of our derivation and on which we can do the following considerations:

- performance-wise Fig. 2(e) is completely equivalent to Fig. 2(a), since we only applied twice the invertible operator rule;
- in the equivalent model in Fig. 2(e), the $\hat{x}$ and $\hat{y}$ QAM components are separated and the frequency dependent $SNR(f)$ can be easily evaluated independently on the two components
- thus, we can use Eq. 3 to obtain the resulting SNR on $\hat{x}$ and $\hat{y}$ at the output of the two FFE equalizers.

In particular, the received field after the equalizer, on the two polarizations, can now be written as

$$\begin{bmatrix}E^x(f)\\E^y(f)\end{bmatrix}_{eq} = \begin{bmatrix}E^x(f)\\E^y(f)\end{bmatrix}_{TX} + \boldsymbol{K}(f) \cdot \begin{bmatrix}n^x(f)\\n^y(f)\end{bmatrix} \tag{6}$$

where $n^x(f)$ and $n^y(f)$ are additive white noise components with PSD $N_0$ and:

$$\boldsymbol{K}(f) = \boldsymbol{H}_{sn}(f)^{-1} = \begin{bmatrix}K^{xx}(f) & K^{xy}(f)\\K^{yx}(f) & K^{yy}(f)\end{bmatrix} \tag{7}$$

The last steps towards obtaining spectrally-resolved $SNR$s requires translating Eq. (6) into the related power spectral densities (PSD) for the signals and noises on the two polarizations. To this end, we remind that the PSD of the sum of two statistically independent random processes is equal to the sum

This article has been accepted for publication in IEEE/OSA Journal of Lightwave Technology. This is the author's version which has not been fully edited and content may change prior to final publication. Citation information: DOI 10.1109/JLT.2023.3242329



of the two individual PSDs. In Eq. (6), the useful signal terms can be considered statistically independent from the noise and, moreover, the two noise components $n^x(t)$ and $n^y(t)$ are also mutually statistically independent. Thus, considering also the well-known formula for the PSD at the output of a linear transfer function, we have:

$$\begin{bmatrix} P^x(f) \\ P^y(f) \end{bmatrix}_{eq} = \begin{bmatrix} P^x(f) \\ P^y(f) \end{bmatrix}_{TX} + \begin{bmatrix} |K^{xx}(f)|^2 + |K^{xy}(f)|^2 \\ |K^{yx}(f)|^2 + |K^{yy}(f)|^2 \end{bmatrix} \cdot N_0 \quad (8)$$

From these equations, we can now derive the spectrally-resolved $SNR$s on the two polarizations:

$$SNR_x(f) = \frac{P^x_{TX}(f)}{(|K^{xx}(f)|^2+|K^{xy}(f)|^2)\cdot N_0}$$
$$SNR_y(f) = \frac{P^y_{TX}(f)}{(|K^{yx}(f)|^2+|K^{yy}(f)|^2)\cdot N_0} \quad (9)$$

This is the main result of our paper, since it allows to analytically derive the spectral $SNR(f)$ on each of the two $\hat{x}$ and $\hat{y}$ useful signal components, which can finally be inserted into Eq. (2) and then into Eq. (1) to estimate the $SNR_x$ and $SNR_y$ metrics on each of the two QAM signals and, consequently, the two resulting $BER$s. This last step is trivial, since under Gaussian assumption the $BER$ vs. $SNR$ relation for each M-QAM format is well know [14] and given by

$$BER = \frac{4}{log_2(M)}\left(1 - \frac{1}{\sqrt{M}}\right)\frac{1}{2}\text{erfc}\left(\sqrt{\frac{3\cdot SNR}{2(M-1)}}\right) \quad (10)$$

where $M$ is the constellation size. The SNR is modulation-format agnostic and thus our analysis applies to a broad range of modulation formats, including higher order QAM, with the same estimation accuracy, provided that the proper BER vs. SNR formula is introduced for each modulation format.

## III. Application Examples and Model Accuracy

In this Section, we introduce two possible scenarios where our model can be applied for fast system performance analysis. On each of the two scenarios, we validate our analytical model comparing its performance estimation with those of detailed time-domain simulations.

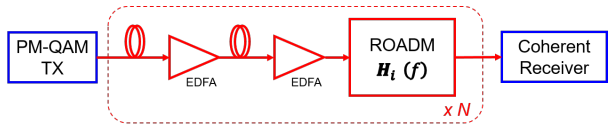


Fig. 3. General schematic considered in Subsection III-A for the scenario of long-haul ROADM-based links.

### A. Long-haul core-network application scenario

In the first scenario, we study the impact of ROADMs [15] with non ideal frequency and polarization dependent transfer functions, a realistic and very common situation for today's wavelength routed optical core and metro networks. In particular, as shown in Fig. 3, we consider the evolution of a PM-QAM signal trough a cascade of EDFAs and $N$ ROADMs, each containing 2 wavelength selective switches (WSS) described by a Super-Gaussian (SG) profile of order 6 as in state-of-the-art MEMS mirror-based WSS [16]. When also considering the effect of PDL and fiber random birefringence, each filtering element can be characterized as:

$$\boldsymbol{H}(f) = \left\{ \begin{bmatrix} H^x(f) & 0 \\ 0 & H^y(f) \end{bmatrix} \begin{bmatrix} 1 & 0 \\ 0 & k \end{bmatrix} \begin{bmatrix} J^{xx} & J^{xy} \\ J^{yx} & J^{yy} \end{bmatrix} \right\}_{xN} \quad (11)$$

where $H^x(f) = H^y(f)$ are the WSS supergaussian profiles on the two polarization axes, $J^{xx}$, $J^{xy}$, $J^{yx}$ and $J^{yy}$ are the four components of a generic [2x2] random unitary Jones matrix and $k = 10^{-\frac{PDL_{dB}}{20}}$, where the PDL is defined as the difference between the maximum and minimum loss on all possible polarization states. Although WSS in modern optical networks can show typical PDL values of 0.5 dB per unit [17], we tested our model in a more challenging scenario and in the following numerical example, we assume $PDL_{dB} = 1$ dB for each individual WSS. Thus, the obtained accuracy is expected to be equal (or even better) in more practical environments where the bandwidth limitation introduced by WSSs with lower PDL is less severe.

Both $\boldsymbol{H}_s(f)$ and $\boldsymbol{H}_n(f)$ are generated as in Eq. 11, with the same supergaussian profiles, the same PDL but independent unitary Jones matrices (to take into account random fiber birefringence). They are normalized to their maximum at $f = 0$ $Hz$, thus their relation to the total signal power is always fixed. The individual filter bandwidth is set to 75 $GHz$ in accordance to FlexGrid spectral arrangement to accomodate a 64 $GBaud$ PM-16QAM signal with raised cosine shaping with 0.2 roll-off factor. Considering a 27% overhead FEC, the net bit rate in our numerical example is about 400 $Gbit/s$. To take into account non-perfect WSS frequency alignment, the central frequency of each WSS is varied randomly in a range included within ±5% of the filter bandwidth and the number of cascaded WSS is set to 10 (i.e. 5 ROADMs with 2 WSS each). We intentionally select parameters that generate very strong polarization and frequency dependent effects, and consequently a large output $SNR$ difference on the two polarizations, to validate our model under somehow extreme conditions. To focus on the target of our model (i.e. the ability to take into account generic polarization and frequency dependent transfer functions) we neglect other impairments, such as fiber nonlinearities but, as already mentioned, the most commonly used models in physical layer aware network planning tools are able to model fiber nonlinearities as equivalent additive Gaussian noise sources [8], [9].

We evaluated the $SNR$ obtained on the two polarizations and plot in Fig. 4 the resulting minimum and maximum values, comparing the values obtained using our analytical model and those resulting from detailed time-domain simulations on the same setup. Here are some further details on the considered system. The 64 $GBaud$ PM-16QAM signal is filtered by 10 cascaded WSS. Fifty Jones matrices are randomly generated for the signal and the noise independently to emulate 50 different realization of the ROADM-based network. The time domain simulator is based on a MIMO-FFE equalizer including a $T/2$-spaced least mean square (LMS) algorithm with 130 taps running at 2 samples per symbol on a total of about 400000 transmitted symbols. The SNR in the time

This article has been accepted for publication in IEEE/OSA Journal of Lightwave Technology. This is the author's version which has not been fully edited and content may change prior to final publication. Citation information: DOI 10.1109/JLT.2023.3242329



domain simulator is computed as the ratio of the average energy of the signal to the mean square error at the output of the receiver DSP FFE equalizer. We show in Fig. 4a the $SNR$ for each of the 50 random runs and compare analytical and time-domain results, highlighting very small discrepancies. We selected the noise level $N_0$ in order to have $BER = 10^{-2}$ in back-to-back (BtB) conditions, for a BtB $SNR$ of about 14 dB. The $SNR$ of the system shown in Fig. 4a can be much lower due to the overall bandwidth reduction after cascading 10 WSS. Interestingly, the SNR is distributed around the BtB SNR and the maximum SNR value can also be higher. This is attributable to the extra attenuation of the noise on one of the polarizations, due to the PDL introduced by the WSSs.

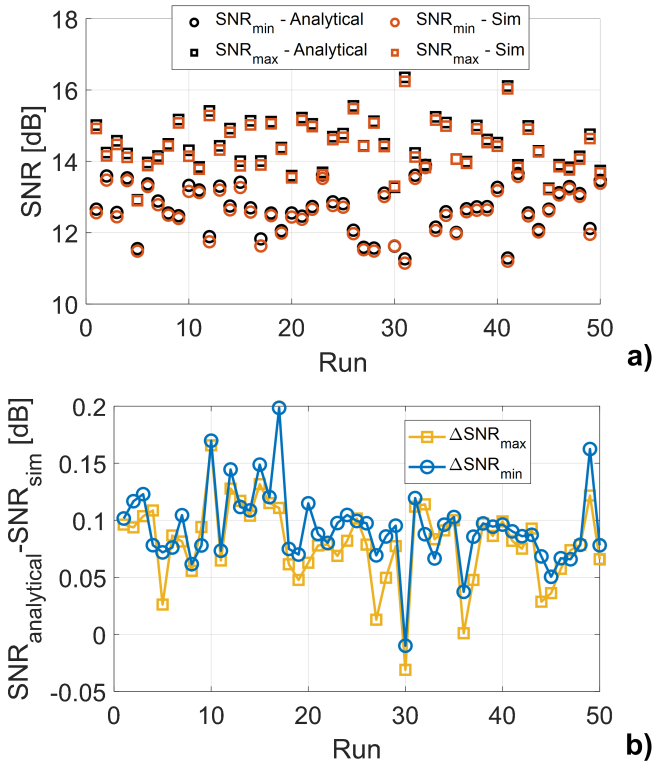


Fig. 4. a) Minimum (circles) and maximum (squares) SNR on each of the two PM signals for a 64 GBaud PM-16QAM signal filtered by 10 WSS, obtained through time-domain simulations (red) and the proposed analytical model (black). b) Difference between SNR obtained through the proposed analytical model and time-domain simulations.

The difference in dB between the $SNR$s computed with the two methods is shown in Fig. 4b. Discrepancies between the two methods of the order of 0.1 dB can be observed, with a maximum of 0.2 dB. As the model is based on the ideal assumption of infinitely long equalization, the difference in Fig. 4b is always positive, thus the analytical model is always conservative as it slightly overestimates the SNR, with the exception of one case (run number 30) where the simulator yields a slightly higher SNR than the model. Nevertheless, the difference is so small that can be attributed to the random statistic of the generated noise vector.

In terms of CPU-time consumption, each time-domain run takes about 16 seconds, whereas the analytical model takes about 0.048 seconds, for a 333 times reduction in computation time that can be crucial in extensive Monte-Carlo modelling for physical layer aware network planning tools.

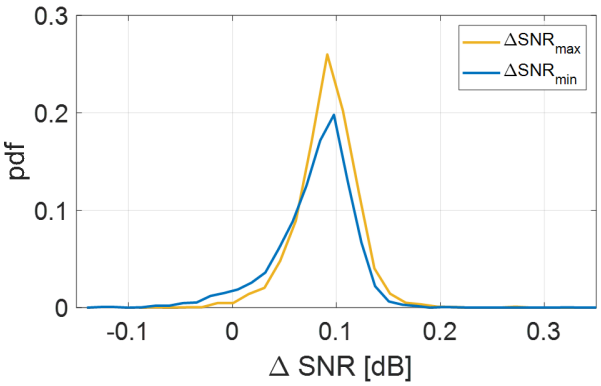


Fig. 5. Probability density function of the error between the analytical model and the time domain simulator for both the maximum (yellow) and minimum (blue) SNR in the ROADM study case, for 3000 runs.

Fig. 5 shows a more comprehensive analysis of the accuracy of the proposed estimation method performed on 3000 randomly generated Monte-Carlo cases. The probability density function (pdf) of the SNR error in dB between the analytical model and the time domain simulator for both the maximum and minimum SNR highlights an average discrepancy of about 0.1 dB in this scenario. Values above 0.2 dB and below -0.05 dB are on the tails of the curves and can be considered statistically negligible. The pdf in Fig. 5 is normalized to the probability so that the sum of all the observations is 1. The results in Fig. 5 confirm "a posteriori" that all assumptions introduced in our model are acceptable and lead to negligible numerical differences to the more complete time domain simulations. Moreover, The SNR rms error in back-to-back conditions, without any filtering, over 3000 runs, is about 0.02 dB which, deducted from the obtained results further reduces the observed 0.1 dB average difference.

### *B. Short-reach intra data-center application scenario*

As another and completely different application example, we used our model in a less common transmission scenario: in [12], [18] we presented an experimental and statistical analysis of an SMF-MMF-SMF coherent system as a possible future solution for next generation CoD-based intra-datacenter (IDC) links, where the existing MMF infrastructure of a data center can be reused in combination with coherent technology to overcome the speed limitations imposed by traditional intensity modulation and direct detection- (IMDD-) based solutions. In this context, we assume that the coherent transceiver developed for this application will still be coupled to a short piece of SMF both at the transmitter output and at the receiver input. In this configuration, we showed in [12], [18] that only the fundamental $LP_{01}$ mode can propagate along the SMF sections, but even under quasi-central launch conditions, high order modes can be excited inside the MMF. In this situation, the resulting end-to-end transfer function becomes strongly polarization and frequency dependent due to

This article has been accepted for publication in IEEE/OSA Journal of Lightwave Technology. This is the author's version which has not been fully edited and content may change prior to final publication. Citation information: DOI 10.1109/JLT.2023.3242329



the relative delays of the MMF modes and to the birefringence seen by each MMF mode, as we demonstrated in [12], [18].

It can be shown that the relation between the $\vec{E}_{TX}$ field of the $LP_{01}$ mode of the first SMF fiber (i.e. the signal generated by the coherent transmitter) and the $\vec{E}_{RX}$ field at the output of the last SMF section (i.e. the signal received by the coherent receiver) is:

$$\vec{E}_{RX}(t) = \sum_{j=0}^{M-1} \rho_j^{in} \boldsymbol{J}_j \cdot \vec{E}_{TX}(t-\tau_j)\rho_j^{out} \tag{12}$$

where $M$ is the total number of MMF modes, $j$ is the index of the $j$th MMF mode, $\rho_j^{in}$ is the coupling coefficient between the $LP_{01}$ SMF mode and the $j$th MMF mode, $\rho_j^{out}$ is the coupling coefficient between the $j$th MMF mode and the SMF $LP_{01}$ mode, $\boldsymbol{J}$ is the unitary random Jones matrix that takes into account "per mode" fiber birefringence and $\tau_j$ is the modal delay of the $j$th mode inside the MMF. Without loss of generality, and only to simplify the equations, we referred all delays and birefringence to those of the fundamental $LP_{01}$ mode, therefore $\tau_0 = 0$. Moreover, the $\rho_j$ parameters can be calculated using the analytical model presented in [19] based on the assumption of infinitely parabolic profile of the MMF and on the computation of overlap integrals between the transverse field of each mode in two consecutive fiber sections. The differential modal delays $\tau_j$ in the MMF are taken from the large database of measured modal delays presented in [20] and we assume that modes belonging to the same mode group strongly couple to each other and have the same modal delay. Further details of the SMF-MMF-SMF system and of the developed model can be found in [12]. By Fourier transforming Eq. (12), we observe that the transmitted signal undergoes the following [2x2] frequency-dependent transfer function matrix:

$$\boldsymbol{H}(f) = \sum_{j=0}^{M-1} \rho_j^{in} \boldsymbol{J}_j e^{-j2\pi f \tau_j} \rho_j^{out} \tag{13}$$

We now apply the analytical model presented in Section II to estimate the SNR of polarization multiplexed coherent systems whose transfer function, defined in Eq. (13), is affected by strong frequency dips due to modal delay and birefringence in a MMF. To do so, we generate 3000 frequency responses by randomly generating Jones matrices for each mode of the MMF, and we compare the results obtained analytically to the output of the time domain simulator based on bit error counting. We assume again that $H_T(f)$ is a squared root raised cosine filter with 0.2 roll-off factor.

As an example, Fig. 6 shows the results obtained through the analytical model compared to the time-domain simulations, for a 25 $GBaud$ PM-16QAM SMF-MMF-SMF system with 100 $m$ MMF fiber with 50 $\mu m$ core diameter and 50 randomly generated Jones matrices accounting for variable birefringence. In Fig. 6a both the minimum and maximum SNR values are shown, highlighting small discrepancies between the two methods. Modal dispersion changes the way all the modes inside the MMF couple to the $LP_{01}$ of the output SMF. This sort of interferometric effect is scrambled by the randomly

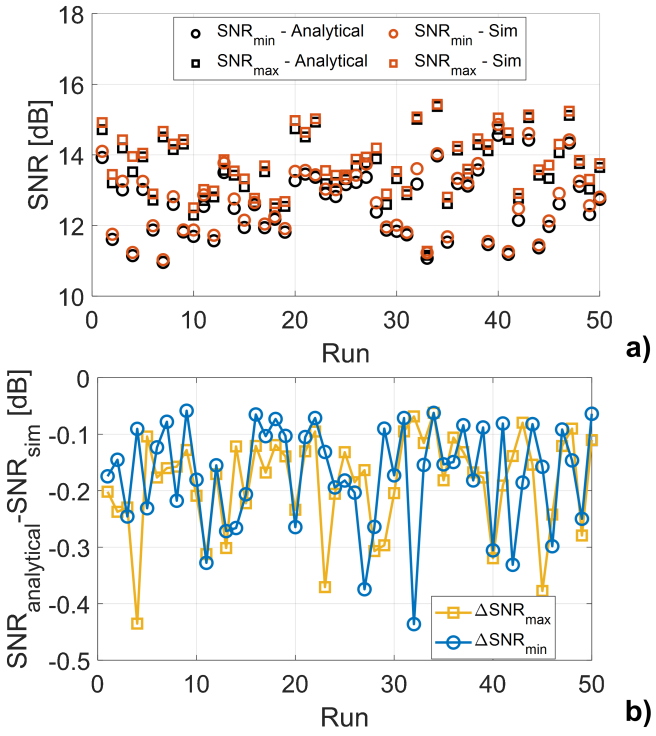


Fig. 6. a) Minimum (circles) and maximum (squares) SNR for a 25 GBaud PM-16QAM SMF-MMF-SMF configuration with 100 m MMF fiber and no MMF-MMF connectors, obtained through time-domain simulations (red) and the proposed analytical model (black). b) Difference between SNR obtained through time-domain simulations and the proposed analytical model.

generated birefringence and causes the SNR to fluctuate. Moreover, the polarization dependence in this case is not due to the PDL introduced by the system components, but to the intrinsic propagation effects of the MMF, where different modes experience different birefringence. The matrix in Eq. 13 is not unitary, even though each Jones matrix $J_j$ is unitary, and this results in an equivalent PDL [12] that can be quite high in this extreme scenario. The obtained PDL is 7.5 dB, on average over 3000 Monte-Carlo cases. Over the considered 50 runs, the SNR varies by more than 3.5 dB. As shown in Fig. 6b, for most of the 50 runs (about 80% of the cases), the analytical model yields less than 0.25 dB error with respect to the simulations in the time domain. For 98% of the cases the error is less than 0.4 dB.

The results of the statistical analysis over 3000 realizations of the SMF-MMF-SMF coherent system are shown in Fig. 7. The distribution of the difference between the proposed analytical tool and the simulator for both the maximum and minimum SNR highlights a similar behaviour as the one of Fig. 5 with the absolute error peaking at about 0.1 dB. However in this case the maximum SNR difference represented by the pdf tails can be sligthly higher. Please note that in both considered scenarios the DSP parameters are fixed for all the 3000 Monte-Carlo runs and in some cases might not be optimal, especially when the channel transfer function frequency dependence is strong, i.e. when the bandwidth limitations or the frequency dips are severe.

This article has been accepted for publication in IEEE/OSA Journal of Lightwave Technology. This is the author's version which has not been fully edited and content may change prior to final publication. Citation information: DOI 10.1109/JLT.2023.3242329



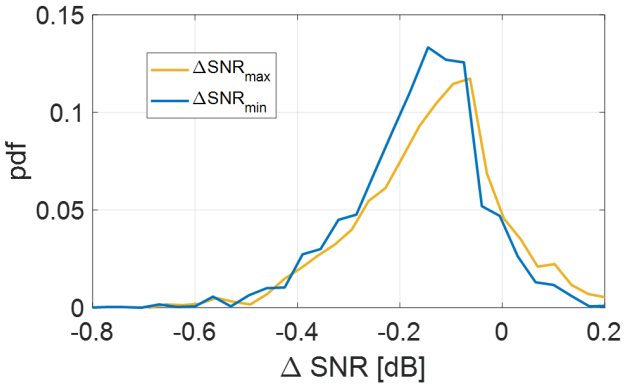


Fig. 7. Probability density function of the error between the analytical model and the time domain simulator for both the maximum (yellow) and minimum (blue) SNR in the SMF-MMF-SMF study case, for 3000 runs.

Moreover, in this specific application example, we observe that the estimated output SNR is in some cases sligthly worse than that computed in the time domain. This can be explained by looking at the four frequency response components reported in Fig. 8 for one of the cases where the SNR error is about 0.5 dB (solid curves). These graphs show important frequency dips in the channel transfer functions, down to less than -15 dB for the $H_{xy}$ and $H_{yx}$ components. For these situations and at around the frequency of the dips, the transfer functions are thus quite close to zero, so that the invertible matrix assumption (which is at the basis of the derivation in Sect. II) is sort of borderline. In these situations, the time-domain simulator has slightly better performance since its adaptive equalizer minimizes the square error on both polarization components simultaneously. On the other hand, the dashed curves (corresponding to one of the cases where the SNR difference is less than 0.05 dB on the two polarizations), show no significant holes in the transfer functions.

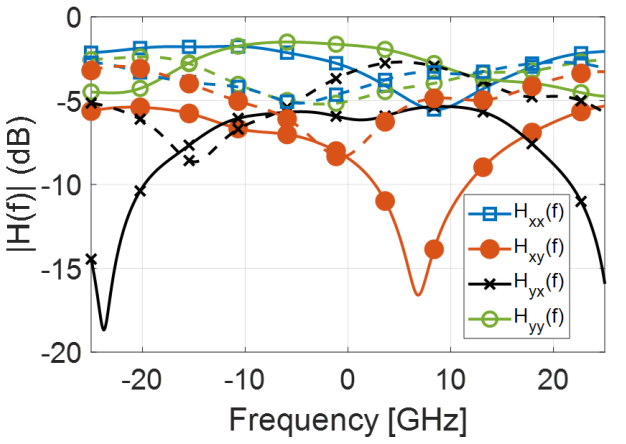


Fig. 8. Examples of the four frequency response components for two cases: solid lines: a critical case when the SNR difference is about 0.5 dB; and dashed lines: a case where the SNR difference is less than 0.05 dB

It should be emphasized that deep frequency dips inside the useful part of the signal spectrum are not typical for "mainstream" coherent systems such as the one discussed in the previous Subsection III-A, so that the issue presented in this paragraph is relevant only in some extreme situations appearing in the somehow exotic coherent-over-MMF links that we presented here only in order to show a completely different application scenario.

## IV. Conclusions

We have presented an analytical model to assess the performance of optical coherent systems for generic polarization and frequency dependence on the transmission channel and generic additive noise. We have evaluated its accuracy compared to much more CPU-time consuming time domain simulations in specific example scenarios. We point out that our model can be applied in several other scenarios. In fact, many modern optical core network planning tools [6] are today based on equivalent linear models where it can be useful to consider polarization and frequency dependence.

In this manuscript, we have applied our analytical model to a system made of 10 cascaded WSS and to an MMF-based system, both described by [2x2] transfer functions that change with the fiber birefringence generated through random unitary Jones matrices. Also, we have focused on two somewhat extreme situations where the system frequency response is severely affected by PDL in the first study case and by mode dispersion in the second. Thus, for a fairer comparison between the (ideal) analytical model and the time domain simulations we neglected the impact of non-ideal features such as other hardware and DSP limitations. Our findings show very good prediction accuracy of our model, with average SNR estimations error of the order of 0.1 dB in both the ROADM and the SMF-MMF-SMF scenarios. The advantage of our analytical approach in terms of prediction speed has also been evaluated, showing reduced CPU time by a factor of more than 300 in both application examples, which highlight the main rationale of our proposal. In fact, in modern physical-layer aware optical network planning tools the speed of execution for forecasting the performance of a set of end-to-end optical lightpaths is key.

## Acknowledgment

*This work was carried out under a research contract with Cisco Photonics and in the PhotoNext initiative at Politecnico di Torino. www.photonext.polito.it*

## References

[1] X. Zhou, R. Urata and H. Liu, "Beyond 1 Tb/s Intra-Data Center Interconnect Technology: IM-DD OR Coherent?," *J. Lightwave Technol.*, vol. 38, no. 2, pp. 475-484, Jan. 2020.

[2] Ezra Ip, Alan Pak Tao Lau, Daniel J. F. Barros, and Joseph M. Kahn, "Coherent detection in optical fiber systems," *Opt. Express*, vol. 16, no. 2, pp. 753-791, 2008.

[3] G. Rizzelli, A. Nespola, S. Straullu, F. Forghieri and R. Gaudino, "Scaling Laws for Unamplified Coherent Transmission in Next-Generation Short-Reach and Access Networks," *J. Lightwave Technol.*, vol. 39, no. 18, pp.5805-5814, 2021.

[4] P. Torres-Ferrera, F. Effenberger, M. S. Faruk, S. Savory and R. Gaudino, "Overview of High-Speed TDM-PON beyond 50 Gbps per Wavelength using Digital Signal Processing [Invited tutorial]," *J. Opt. Commun. Netw.*, vol. 14, no. 12, pp. 982-996, 2022.

[5] S. J. Savory, "Digital Coherent Optical Receivers: Algorithms and Subsystems," *IEEE J. Sel. Top. Quantum Electron.*, vol. 16, no. 5, pp. 1164-1179, Sept.-Oct. 2010.

[6] A. Ferrari, M. Cantono, A. Ahmad and V. Curri, "Physical layer strategies to save lightpath regenerators," *J. Opt. Commun. Netw.*, vol. 10, no. 9, pp. 703-711, Sept. 2018.

[7] R. -J. Essiambre, G. Kramer, P. J. Winzer, G. J. Foschini and B. Goebel, "Capacity Limits of Optical Fiber Networks," *J. Lightwave Technol.*, vol. 28, no. 4, pp. 1164-1179, pp. 662-701, Feb., 2010

[8] V. Curri, M. Cantono and R. Gaudino, "Elastic All-Optical Networks: A New Paradigm Enabled by the Physical Layer. How to Optimize Network Performances?," *J. Lightwave Technol.*, vol. 35, no. 6, pp. 1211-1221, 15 March, 2017.

[9] P. Poggiolini, "The GN Model of Non-Linear Propagation in Uncompensated Coherent Optical Systems," *J. Lightwave Technol.*, vol. 30, no. 24, pp. 3857-3879, Dec.15, 2012.

[10] Robert F.H. Fischer, "Linear Equalization," in *Precoding and Signal Shaping for Digital Transmission*, New York, NY, USA: Wiley-Interscience, 2002, ch. 2, sec. 2.2.4, pp. 35-43.

[11] G. D. Forney and G. Ungerboeck, "Modulation and coding for linear Gaussian channels," *IEEE Transactions on Information Theory*, vol. 44, no. 6, pp. 2384-2415, Oct. 1998.

[12] G. Rizzelli, P. Torres-Ferrera, F. Forghieri, A. Nespola, A. Carena and R. Gaudino, "Coherent Communication Over Multi Mode Fibers for Intra-Datacenter Ultra-High Speed Links," in *Journal of Lightwave Technology*, vol. 40, no. 15, pp. 5118-5127, 1 Aug.1, 2022.

[13] J. G. Proakis and M. Salehi, "Optimum Receivers for AWGN Channels," in Digital Communications, fifth ed. New York, NY, USA: McGraw-Hill, 2008, ch. 4, sec. 4.1, pp. 166-167.

[14] K. Cho and D. Yoon, "On the general BER expression of one- and two-dimensional amplitude modulations," in *IEEE Transactions on Communications*, vol. 50, no. 7, pp. 1074-1080, July, 2002

[15] A. Abdo and C. Damours, "Performance of LMS Based Adaptive Filtering in Coherent Optical Receivers in Presence of State-of-Polarization Transients, PDL and ROADMs," in *Proc. CCECE*, Quebec City, Canada, 2018.

[16] F. Heismann, "System requirements for WSS filter shape in cascaded ROADM networks," in *Proc. OFC*, San Diego, CA, USA, 2010.

[17] A. Dumenil, E. Awwad and C. Méasson, "Polarization Dependent Loss: Fundamental Limits and How to Approach Them," in *Proc. Advanced Photonics*, New Orleans, LA, USA, 2017.

[18] G. Rizzelli, F. Forghieri and R. Gaudino, "Experimental Demonstration of Real-Time 400G Coherent Transmission Over 300m OM3 MMF," in *Proc. OFC*, San Diego, CA, USA, 2022.

[19] A. Amphawan, F. Payne, D. O'Brien and N. Shah, "Derivation of an Analytical Expression for the Power Coupling Coefficient for Offset Launch Into Multimode Fiber," *J. Lightwave Technol.*, vol. 28, no. 6, pp. 861-869, March 15, 2010.

[20] P. Torres-Ferrera et al., "Statistical Analysis of 100 Gbps per Wavelength SWDM VCSEL-MMF Data Center Links on a Large Set of OM3 and OM4 Fibers," *J. Lightwave Technol.*, vol. 40, no. 4, pp. 1018-1026, Feb. 15, 2022.